frontiers in Physics

ORIGINAL RESEARCH
published: 13 May 2021
doi: 10.3389/fphy.2021.674958

Effect of F-Actin Organization in Lamellipodium on Viscoelasticity and Migration of Huh-7 Cells Under pH Microenvironments Using AM-FM Atomic Force Microscopy

Miao Chen[1,2,3], *Wenpeng Zhu*[1,2,3]*, *Zhihua Liang*[1,2,3], *Songyou Yao*[1,2,3], *Xiaoyue Zhang*[1,2,3]* *and Yue Zheng*[1,2,3]

[1]School of Physics, Sun Yat-sen University, Guangzhou, China, [2]State Key Laboratory of Optoelectronic Materials and Technologies, Sun Yat-sen University, Guangzhou, China, [3]Centre for Physical Mechanics and Biophysics, School of Physics, Sun Yat-sen University, Guangzhou, China

OPEN ACCESS

Edited by:
Ying Li,
University of Connecticut, United States

Reviewed by:
Zhao Qin,
Syracuse University, United States
Lei Tao,
University of Connecticut, United States

***Correspondence:**
Wenpeng Zhu
zhuwp3@mail.sysu.edu.cn
Xiaoyue Zhang
zhangxy26@mail.sysu.edu.cn

Specialty section:
This article was submitted to Biophysics, a section of the journal Frontiers in Physics

Received: *02 March 2021*
Accepted: *29 April 2021*
Published: *13 May 2021*

Citation:
Chen M, Zhu W, Liang Z, Yao S, Zhang X and Zheng Y (2021) Effect of F-Actin Organization in Lamellipodium on Viscoelasticity and Migration of Huh-7 Cells Under pH Microenvironments Using AM-FM Atomic Force Microscopy. Front. Phys. 9:674958. doi: 10.3389/fphy.2021.674958

Cytoskeleton is responsible for fundamental cellular processes and functions. The filamentous actin (F-actin) is a key constituent of the cytoskeleton system which is intrinsically viscoelastic and greatly determines the mechanical properties of cells. The organization and polymerization of F-actin are relevant to the viscoelasticity distribution and the migration of living cells responding to pH microenvironments. Recently, progression in various diseases such as cancers have been found that cellular migration is related to the alterations in the viscoelasticity of lamellipodium. However, the correlation among F-actin organization, viscoelastic properties and cellular migration of living cancer cells under different pH microenvironments are still poorly understood. Conventional experimental methods of optical microscopy and atomic force microscopy (AFM) can neither break the trade-off between resolution and rate in cytoskeleton imaging, nor achieve the structural characterization and the mechanical measurement simultaneously. Although multifrequency AFM with amplitude modulation-frequency modulation (AM–FM) enables us to probe both the surface topography and the viscoelasticity distribution of cells, it is difficult to image the cytoskeletal filaments with the diameter down to the scale of tens of nanometers. Here, we have improved the AM-FM AFM by employing the high damping of cell culture medium to increase the signal-to-noise ratio and achieve a stable imaging of F-actin with the resolution down to 50 nm under *in situ* microenvironment. The approach that can successfully visualize the structures of cytoskeletal filaments and measure the distribution of mechanical properties simultaneously enable us to understand the relationship between the organization of F-actin and the viscoelasticity of living Huh-7 cancer cells under different pH values. Our experimental results have demonstrated that, unlike the randomly distributed F-actin and the homogeneous viscoelasticity at the normal pH level of 7.4, the living Huh-7 cancer cells with the reduced pH level of 6.5 show highly oriented and organized F-actin along the lamellipodium direction associated with the significant gradient increase both in elasticity and viscosity, which are confirmed by immunofluorescence confocal microscopy. The F-actin organization and the gradient

viscoelasticity of lamellipodium provide structural and mechanical understanding on the adhesion and migration of living cancer cells that undergo metastasis and malignant transformation.

Keywords: amplitude modulation-frequency modulation atomic force microscopy, living cancer cells, viscoelasticity gradient, F-actin cytoskeleton, lamellipodium, pH microenvironments, migration

INTRODUCTION

Living cells, as the smallest unit in biological systems, plays a pivotal role in human life and disease processes [1]. Changes in the viscoelastic properties of cells are relevant to the fundamental cellular physiological behaviors and functions, such as cell migration [2], adhesion [3], differentiation [4] and absorption [5]. Cytoskeleton that is an essential structural component of cells, is intrinsically viscoelastic and responsible for the cell viscoelasticity [6], controlling the cellular development and maintenance [7]. In the cytoskeleton system, the filamentous actin (F-actin) (**Figure 1**) is one of the most major constituent building up many higher order structures in cells (e.g., stress fibers, lamellipodia, and filopodia) [8]. The arrangement and distribution of F-actin greatly dominates the mechanical properties of cells including viscoelasticity [9–13]. For example, the actin cortex is a thin layer that lies beneath the plasma membrane, maintaining and regulating cell topography [10]. Oberleithner et al. found that the depolymerization of cortical actin induced by altering the local microenvironment reduces the elasticity of cells, thus modulating the deformation of the plasma membrane [11]. The stress fibers are arranged in parallel by F-actin, connecting the cytoskeleton to the extracellular matrix via focal adhesions [12]. Wang et al. reported that viscosity of F-actin can significantly increase stability of the cell adhesion [13]. The cellular protrusions including lamellipodium and filopodium located at the edge of cells is involved with the cell migration [14, 15]. Lamellipodia are sheet-like structures, from which filopodia usually grow out [16]. Lamellipodial branched actin network not only generates a pushing force by actin polymerization but also provides crucial mechanical support for cell migration through the extracellular matrix or adjacent cells [17, 18]. Laurent et al. revealed that cells migrates toward the more rigidity side of the lamellipodia [19]. Moreover, lamellipodia-based cell migration plays a crucial role in cancer metastasis [20]. The malignant degree of cancer cells is related to their migration speed, that is, the metastasis and invasiveness of cancer cells [21]. In particular, in the complex microenvironment of tumor tissues [22, 23], the cancer cells will change the structure and topography of lamellipodia at an acid pH level, and then accelerate their metastasis [24, 25]. However, the organization of the F-actin in lamellipodia under different pH microenvironments associated with the underlying relationship with the viscoelasticity and migration of living cancer cells remain unclear and is in urgent need to be fully interpreted. The nanomechanical mechanism revealing the effects of F-actin in lamellipodia on the cell viscoelasticity and migration represents a meaningful approach to understand the physical nature in the malignant metastasis of cancer cell response to the change of pH microenvironments.

To understand the correlation among F-actin organization, viscoelastic properties and cellular migration of living cancer cells under different pH microenvironments, it is the key issue to simultaneously obtain the high-resolution *in situ* images of the cytoskeleton topography and viscoelastic properties of cells. For the soft matter of cells that are heterogeneous with intrinsically

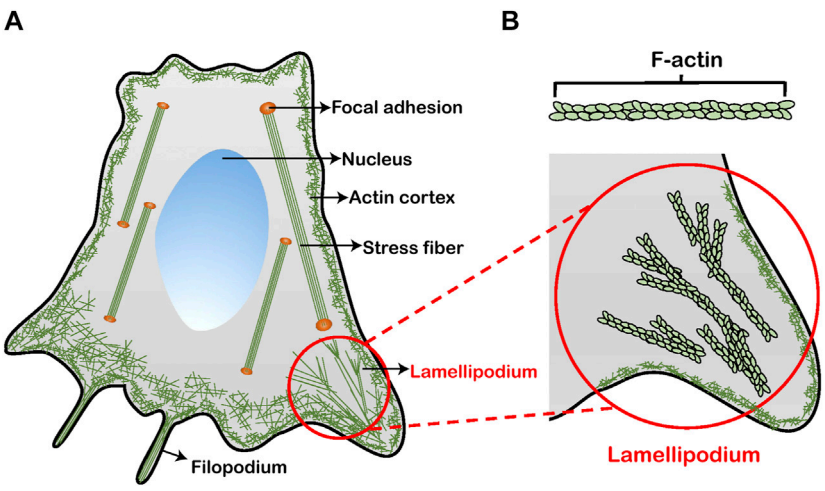

FIGURE 1 | Schematics of a cell with F-actin architectures. **(A)** Four primary types of F-actin structures in the cytoskeleton: actin cortex, stress fiber, filopodium, and lamellipodium. **(B)** A magnified view of the lamellipodium. The formation of lamellipodium is facilitated by the organization of F-actin.

viscoelastic cytoskeletons and undergo large deformation [26, 27], the structural organization and mechanical properties are highly coupled [28]. A wide variety of experimental work has been performed in order to assess the relationship between cell mechanics and microstructures [29, 30], focusing on the changes in either cytoskeletal structure [29] or elasticity [30]. However, these experiments have been limited by the characterization methods of cells and cytoskeletons. Although the fluorescence imaging techniques have the advantage in the fast *in situ* identification of subcellular structures, it is difficult for the optical resolution to be smaller than the diffraction limit around hundreds of nanometers and capture the details of cytoskeletal structures [31]. The transmission electron microscopy is usually adopted to observe the cells and cytoskeletons [32]. Nevertheless, the sample preparation process is complicated with fixation, dehydration, infiltration and staining, which will cause the loss of cell activity [33]. Furthermore, the imaging of transmission electron microscopy is slow and commonly conducted under vacuum condition, which make it unable for the fast *in situ* identification of cells and cytoskeletons under different microenvironments. For studying cellular mechanics, a number of experimental methodologies have been developed, including micropipette aspiration [34], traction force microscope [35], optical tweezers [36], and magnetic twisting cytometry [37]. Atomic force microscopy (AFM) is one of the most major and reliable methods for probing the mechanical properties of cells [38, 39]. Conventional AFM imaging based on contact mode force curve measurement has been introduced to measure the cellular viscoelasticity [40, 41]. And yet the poor resolution and long acquisition time prevent it from fast high-resolution characterization of subcellular microstructures and mechanical properties. It is a key challenge to not only break the trade-off between resolution and rate in cytoskeleton imaging, but also achieve the structural characterization and the mechanical measurement simultaneously.

In this work, we use amplitude modulation–frequency modulation (AM–FM) AFM to characterize the topography and viscoelasticity of living Huh-7 cancer cells at the same time. We have improved the AM-FM AFM by using the high damping of cell culture medium, instead of original damping materials that cannot be used in liquid, to dissipate unnecessary vibration that deviates from the standard resonance of the AFM cantilever. The efficient stabilization of the cantilever oscillation enables us to increase the signal-to-noise ratio, achieving a fast imaging and mapping simultaneously of F-actin structures, cellular topography and viscoelasticity with the ultrahigh resolution down to 50 nm under *in situ* pH microenvironment. Moreover, the capability of AM–FM AFM to capture the F-actin microstructures are validated by immunofluorescence confocal microscopy. By using AM–FM AFM, we study the effect of pH level on the organization of F-actin in lamellipodium and the change in the topography and viscoelasticity of living Huh-7 cancer cells. The experimental results demonstrate that the F-actin in lamellipodium under normal culture medium (pH 7.4) is short, thin and dispersed, associated with the homogeneous distribution of cell viscoelasticity. On the contrary, in acid culture medium (pH 6.5), the F-actin cytoskeletons polymerize and are woven into a long and thick bundle-like structure directed to the protruding direction of lamellipodium. Both the elasticity and viscosity show a significant gradient increase along the protruding direction, which can facilitate the adhesion and migration of living cancer cells. These results have significant implications for understanding the significance of F-actin structures and viscoelasticity in changing cell topography and behaviors, and opening a new paradigm of nanomechanical mechanisms for the metastasis of cancer cells under pH microenvironments.

MATERIALS AND METHODS

Cells Culture and Treatment

The cells used in this study are the human hepatoma cell lines Huh-7 cells, obtained from the Type Culture Collection of the Chinese Academy of Sciences, Shanghai, China. The cells were cultured in Dulbecco's Modified Eagle Medium (Gibco, Life Technologies, China) supplemented with 10% fetal bovine serum (Gibco, Life Technologies, Australia) and 1% penicillin-streptomycin (Gibco, Life Technologies, United States), at 37°C and 5% CO_2 in humid conditions. The pH level of normal culture medium is set as 7.4. One day prior to the AFM experiments, the cells were seeded onto 25 mm × 25 mm glass slides. After the cells had enough time to adhere to the substrate, the existing medium was replaced with the fresh medium to remove dead and loosely attached cells every 2 h. The fresh medium was prepared in the normal or acid condition to mimic microenvironments at different pH levels. HCl (0.5 mol/L) was added precisely to the normal culture medium for the acid culture medium (pH 6.5) by using a pH meter measurement to verify the targeted pH value of 6.5. Phosphate buffer saline (PBS) solution was used to rinse the substrate every time before adding and changing the culture medium. The cells were cultured with either pH microenvironment for at least 6 h in CO_2 incubator for subsequent characterization and measurement in AFM experiments. To maintain the pH level in the cell cultivation, the new acid culture medium of pH 6.5 was replaced every 2 h. By pH monitoring, we found that the acid culture medium of pH 6.5 in the CO_2 incubator can be kept well within 2 h. The time of AM-FM AFM measurement was limited to a maximum of 2 h. During the AM-FM AFM measurement, the pH monitoring was employed constantly and the acid culture medium of pH 6.5 was added when needed.

Atomic Force Microscopy

AFM experiments were performed with an Asylum Research MFP-3D Infinity AFM system. The AM-FM bimodal imaging mode was performed by using BL-AC40TS cantilever (Olympus, Japan) with 0.11 nN/nm nominal force constant (k_1). The spring constant for the first eigenmode k_1 of the cantilever was obtained by force constant calibration. In AM-FM method that employs the tapping mode, the cantilever is excited near the first and second resonant frequencies simultaneously. To ensure the physiological conditions of cells, the cantilever was completely

immersed in the liquid of culture medium during the experiments. The cantilever tuning was conducted in liquid by which the first cantilever eigenmode was excited to the resonant frequency ($f_1 \approx 30$ kHz) by the AFM software (Asylum Research) and the second eigenmode to the second-order resonant frequency ($f_2 \approx 110$ kHz). And the spring constant for the second eigenmode k_2 of the cantilever can be calculated by $k_2 = \left(\frac{f_2}{f_1}\right)^2 k_1$.

During the scanning, the first order amplitude A_1 is adjusts to maintain constant that is equal to amplitude setpoint $A_{1,\text{set}}$, so that the displacement of scanner in z-direction can be used for living cell topography tracking. Meanwhile, the cantilever is also excited at the second resonant frequency f_2. Here, a frequency feedback loop adjusts the frequency by a small amount Δf_2 to maintain the second eigenmode on resonance as the AFM tip interacts with the cell. The AM-FM signals were recorded by the lock-in and feedback system and can be used to extract the effective storage modulus E_{storage} for elastic property [42]:

$$E_{\text{storage}} = \frac{\pi}{R}\sqrt{\frac{1}{6}}\left(\frac{k_1}{Q_1}\frac{A_{1,\text{free}}}{A_{1,\text{set}}}\cos\varnothing_1\right)^{-\frac{1}{2}}\left(\frac{2k_2\Delta f_2}{f_2}\right)^{\frac{3}{2}},$$

where Q_1 are the quality factor, $A_{1,\text{free}}$ (4.0 V) is the free amplitude tuned for the first eigenmode in liquid, $A_{1,\text{set}}$ (2.0 V) is the setpoint used for imaging, and R (~10 nm) is the radius of AFM tip provided by the manufacturer. As described in details [43], the mapping of loss tangent E_{loss} can be derived by the amplitude (A_1) and phase signals ($\varnothing_1$) in the first resonance mode:

$$E_{\text{loss}} = \frac{\pi\left(\frac{A_{1,\text{set}}}{A_{1,\text{free}}} - \sin\varnothing_1\right)}{\cos\varnothing_1}.$$

The loss tangent is equivalent to the ratio of the dissipated energy to stored energy:

$$\text{Loss tangent} = \frac{E_{\text{loss}}}{E_{\text{storage}}},$$

which allows us to calculate the loss modulus for viscous property. Correlated topography and viscoelastic images were generated with a resolution of 256 × 256 pixels. And the scan speed was set at 0.5 line/s. As the modulus of the AFM tip used defers greatly from that of the glass substrate, the mechanical signal from the background part of glass substrate is meaningless and not considered, and is shown as the gray background in **Figures 4**, **5**. The same AFM tip and imaging configuration were used for all samples to maintain consistency between measurements of cell viscoelasticity. Repetitions of experiments with more living Huh-7 cancer cells under different pH states are performed to verify the robustness of results and mechanisms in our work.

Confocal Fluorescence Microscopy

Confocal fluorescence microscopy was used to observe the F-actin microstructures and validate the AFM imaging. The cells for the imaging by confocal fluorescence microscopy were seeded onto 20 mm cell slides and incubated with the same culture conditions as for AFM measurements. The cells were washed with PBS, fixed with 4% paraformaldehyde in PBS and kept at 4°C for around 15 min. Afterwards the cells were permeabilized with 0.5% Triton X-100 in PBS at room temperature for 15 min and rinsed with PBS. The nucleus of cells was stained with DAPI (Solarbio, China) for 15 min in dark. The F-actin cytoskeleton of cells was stained in dark using Alexa-Fluor 488 Phalloidin (Solarbio, China) for 30 min. Finally, the slides were mounted with the DAPI mounting medium (Solarbio, China). The stained cells were examined by using a confocal microscope setup (Leica SP8X, Germany) to visualize the F-actin microstructures. The fluorescent F-actin cytoskeleton images were acquired with a 63x/1.40 oil immersion objective lens (Leica Microsystems, Germany).

RESULTS AND DISCUSSION

Improved Amplitude Modulation-Frequency Modulation Atomic Force Microscopy for Mapping Topography and Viscoelasticity of Living Cells

To simultaneously obtain the images of topography and viscoelastic properties of living cells under physiological conditions, we have improved the original AM-FM AFM assembly. In the AM-FM method, two driving signals with different frequencies (black and red signals) are superposed to excite two independent vertical oscillation modes of the cantilever (**Figure 2A**). The first resonance operates in normal tapping mode (AM mode). The amplitude A_1 controls the vertical feedback loop of the standard tapping mode for topography, and the phase $\varnothing_1$ gives the values for the loss tangent (black box). The second resonance operates in the FM mode. The change in resonance frequency f_2 determines the elasticity, while the change in the amplitude A_2 gives the dissipation information (red box). Therefore, the AM-FM method strictly relies on the resonance information of the cantilever, and the stability of the first-order and second-order resonance peaks limits the signal-to-noise. Although AFM with AM-FM mode is competent for the simultaneous mapping of topography and viscoelasticity, the original AM-FM AFM of MFP-3D Infinity AFM system is inappropriate for the *in situ* environment of cell culture medium, as the build-in high damping material that is required to optimize the resonance of the cantilever cannot work in the liquid of culture medium. Without the high damping material, it is difficult for AM-FM AFM to achieve high-resolution imaging of F-actin microstructures [44]. In our work of *in situ* AM-FM AFM imaging, we unloaded the original high damping material and naturally used the liquid of cell culture medium as the high damping to dissipate unnecessary vibration in the oscillation process of AFM cantilever that deviates from the standard resonance. **Figure 2B** shows the first resonance signal of the cantilever without high damping in air, while **Figure 2C** shows the first resonance signal of the cantilever with the high damping in liquid. The introduction of

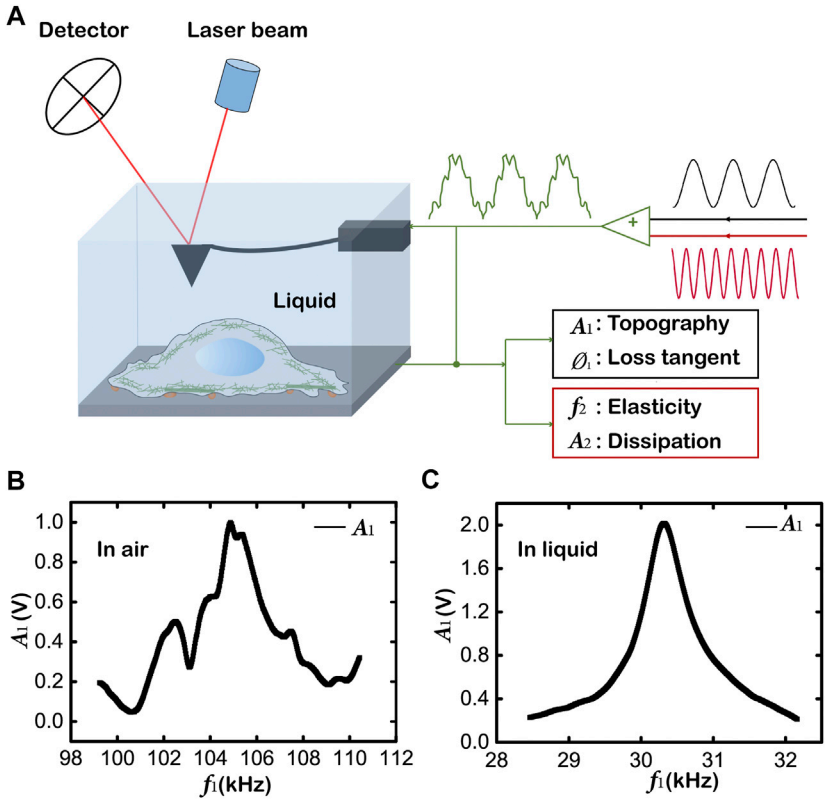

FIGURE 2 | Mapping topography and viscoelasticity of living cells by AM-FM AFM. **(A)** Schematics of the AM-FM AFM showing the experimental setup and the working principle. The AFM tip and the whole cantilever are immersed in the liquid of culture medium for *in situ* measurement of living cells in physiological condition. Two separate excitation signals are combined to excite the cantilever resonances. The cantilever deflection when probing the sample is analyzed to evaluate the offsets of the two resonances for the mapping of topography and viscoelasticity. **(B)** The first resonance signal of the cantilever without high damping in air. **(C)** The first resonance signal of the cantilever in liquid.

the high damping eliminates spurious peaks of the vibration information from unnecessary media and optimizes the resonance of the cantilever to form a clean standard peak in liquid. Similarly, the cluttered signal of the second-order resonance is greatly reduced due to the presence of high damping in liquid (see **Supplementary Figure S1**).

In addition, the ratio $A_{1,\mathrm{set}}/A_{1,\mathrm{free}}$ is set in the range of 0.3–0.5 which ensures the optimal tracking of surface topography for living cell imaging in AM-FM AFM. By introducing the high damping and setting the appropriate parameters, we successfully stabilize the cantilever oscillation, efficiently increase the signal-to-noise ratio, and achieve a high-resolution mapping in AM-FM AFM. As shown in **Figure 3**, we are able to simultaneously measure the cell topography (**Figures 3A,B**), associated with the distributions of storage modulus E_{storage} (**Figure 3C**), loss modulus E_{loss} (**Figure 3D**), and loss tangent (**Figure 3E**) of living cancer cells under physiological conditions. By taking advantage of the high contrast in the mapping of loss tangent, we have achieved an ultrahigh resolution down to 50 nm (**Figure 3F**) and captured cytoskeleton microstructures under *in situ* microenvironment.

Figure 3 shows the topography and viscoelasticity of living cells. It is important to note that the string microstructure observed in the images of viscoelasticity (**Figures 3C–E**) are highly correlated to the features observed in the topography image (**Figures 3A,B**). The widths of the strings are tens of nanometers. The storage moduli E_{storage} of the strings are higher than the gaps in between as shown in **Figure 3C**, while the loss tangents of the strings in **Figure 3E** are lower. These results show that the string microstructure takes the elasticity as the dominant property, which may correspond to the mechanical characteristics of cytoskeletons reported in previous study [45]. Hence, the same topography and viscoelasticity give us a strong implication that the microstructures shown by AM-FM AFM are cytoskeletons, which will be confirmed as F-actin by the latter section of immunofluorescence confocal microscopy. This AM-FM AFM method allows a direct observation in correlation of cytoskeletal structure with both topography and viscoelasticity for living cells, which shows better capability and application than the optical microscope that is limited by the diffraction limit resolution [31], the transmission electron microscope that cannot maintain the physiological state of living cells [32], and other methods for measuring mechanical properties of cells including the traction force microscope, optical tweezers and magnetic twisting cytometry that cannot obtain the topography simultaneously [35–37]. Our improvement of AM-FM AFM

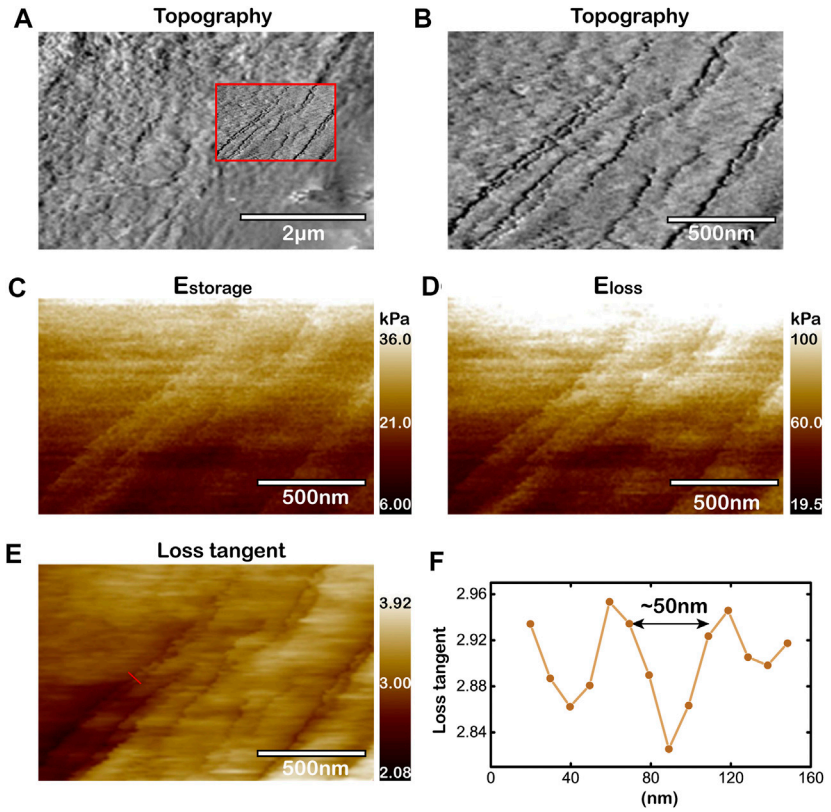

FIGURE 3 | Capability to image cytoskeleton microstructures of living cells by improved AM-FM AFM. **(A,B)** Topography of microregion near the periphery of living cancer cell. The view of **(B)** magnifies the rectangular region within the red box in **(A)**. Topography of the red box in **(A)**. **(C–E)** Mapping of $E_{storage}$ **(C)**, E_{loss} **(D)**, and loss tangent **(E)** simultaneously obtained by AM-FM AFM. **(F)** Cross-section profiles for the loss tangent along the red solid line in **(E)**.

has increased the resolution of cell mechanical imaging, and achieved simultaneously characterization of cytoskeleton topography, viscoelasticity, which are crucial for studying the relationship between the organization of cytoskeleton microstructure and the distribution of mechanical properties associated with their effects on cellular behaviors and functions.

Topography and Viscoelasticity of Cytoskeletons in Lamellipodium at pH 7.4

Based on the *in situ* AM-FM AFM method we improved for simultaneous mapping topography and viscoelasticity of living cells, it is feasible to study the relationship between the organization of cytoskeleton microstructures and the distribution of viscoelastic properties under different pH microenvironments. The microenvironment of cancer cells in tumor tissue is constantly acidified [23], with a lower extracellular pH value (~6.5) than the basic value (~7.4) in normal tissue [22]. The acid microenvironment enables the progression of cancer cells by promoting proliferation, the evasion of apoptosis, metabolic adaptation, migration and invasion that are involved with the malignant transformation and metastasis [46]. During this stage, the F-actin and the lamellipodium are the two crucial media linking the cellular behaviors and the mechanical properties. It has been reported that the acid extracellular pH induces the reorganization of F-actin cytoskeleton and facilitates the formation of lamellipodial protrusion [25], which can modulate the morphology and rigidity against the forces needed for cell migration [47]. It would be a key challenge and a great significance to study the correlation between the organization of F-actin structures and the viscoelasticity distribution in lamellipodium of living cancer cells under normal (pH 7.4) and acid (pH 6.5) microenvironments for revealing the nanomechanical mechanism of the cellular migration in metastasis.

In the normal microenvironment (pH 7.4), we use the improved AM-FM AFM method to characterize the topography and the viscoelasticity of living Huh-7 cells as shown in **Figure 4**. **Figure 4A** shows an overall topography of the cell edge, with the region of lamellipodium in the red box measured by larger contact force and scanning density for higher resolution in topography (**Figure 4B**), storage modulus $E_{storage}$ (**Figures 4C,D**), loss modulus E_{loss} (**Figures 4E,F**), and loss tangent (**Figures 4G,H**). The topography image of **Figure 4B** represents the shot and thin cytoskeletal structures randomly dispersed in lamellipodium, which is also reflected by the

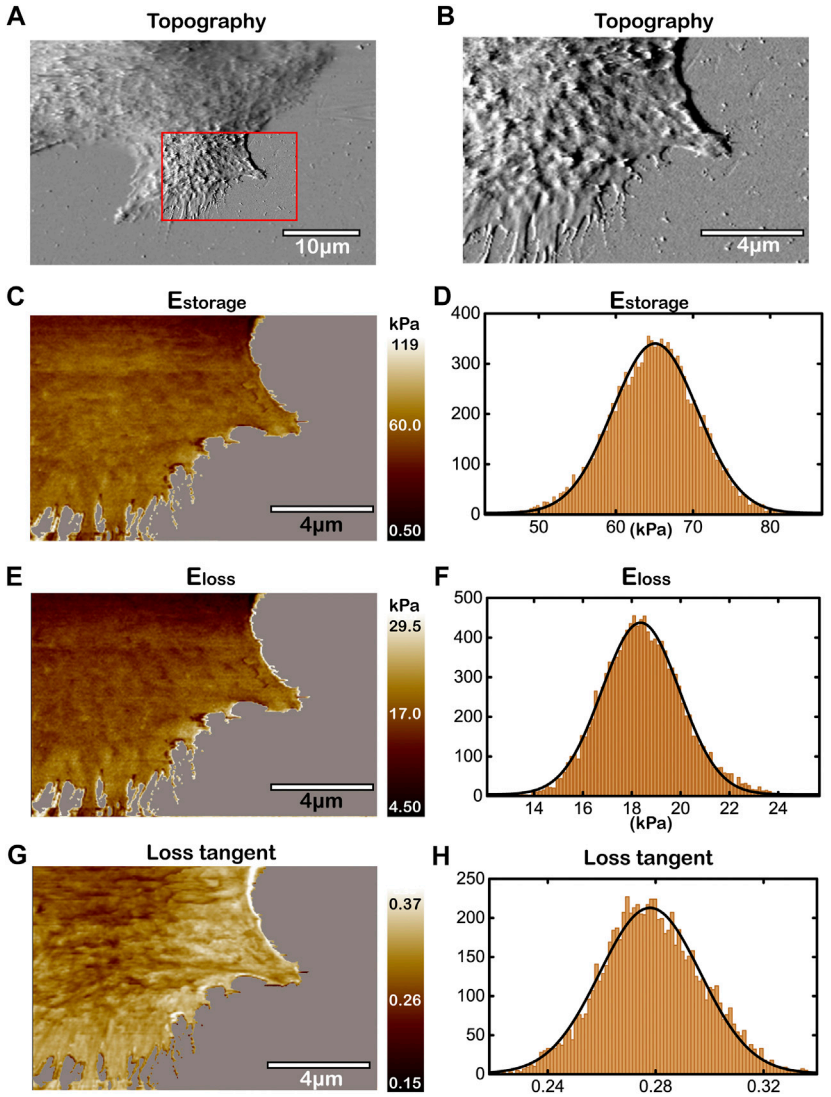

FIGURE 4 | Topography and the viscoelasticity of Huh-7 cells at pH 7.4. **(A)** Topography of cell edge. **(B)** High-resolution topography of lamellipodium region within the red box in **(A)**. **(C**,**E**,**G)** Mapping of $E_{storage}$ **(C)**, E_{loss} **(E)**, and loss tangent **(G)** simultaneously obtained by AM-FM AFM. **(D**,**F**,**H)** Histogram analyses of the measured $E_{storage}$, E_{loss}, and loss tangent in **(C)**, **(E)** and **(G)**, respectively.

homogeneous patterns of viscoelasticity (**Figures 4C,E,G** and **Supplementary Figure S2**). The histogram analyses of storage modulus, loss modulus and loss tangent for **Figures 4C,E,G** were performed as shown in **Figures 4D,F,H**, respectively. The storage modulus in the lamellipodium region (**Figure 4D**) indicates a single Gaussian peak for elasticity with the main range of 50–80 kPa and the mean value of ~65 kPa, which are in good agreement with previous studies [29, 48]. Similarly, the viscous properties measured by loss modulus and loss tangent exhibit monomodal Gaussian peaks, which further indicates the homogeneous distribution of cytoskeletons (**Figures 4F,H**). The Gaussian peak of loss modulus has a mean value of ~18 kPa with the range varying from 14 to 24 kPa, while that of the loss tangent has a mean value of ~0.28. The mappings of storage modulus and loss modulus demonstrate that the cytoskeletons have slightly higher elasticity and viscosity than the background of intracellular fluid or other organelles (**Figures 4C,E**) [48]. Note that the greater difference between the cytoskeletons and the intracellular background is shown in the mapping of loss tangent (**Figure 4G**), owing to the dominant elasticity of cytoskeletal filaments [28, 29]. As a result, the mapping of loss tangent can show higher contrast and resolution with the patterns greatly corelated to the cytoskeletal structures in the topography image, which further proves the capability in characterizing the detailed organization of cytoskeletal structures by the improved AM-FM AFM. Repetitions of experiments for more living Huh-7 cancer cells at pH 7.4 (**Supplementary Figure S2**) show similar cytoskeleton

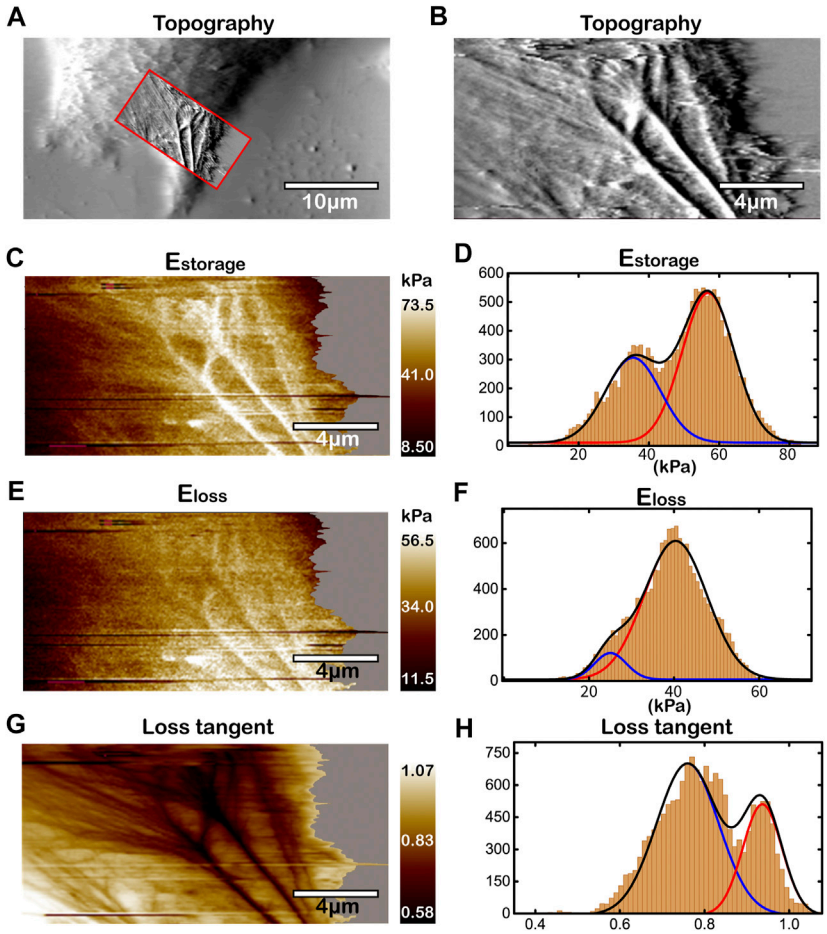

FIGURE 5 | Topography and the viscoelasticity of Huh-7 cells at pH 6.5. **(A)** Topography of cell edge. **(B)** High-resolution topography of lamellipodium region within the red box in **(A)**. **(C**,**E**,**G)** Mapping of $E_{storage}$ **(C)**, E_{loss} **(E)**, and loss tangent **(G)** simultaneously obtained by AM-FM AFM. **(D**,**F**,**H)** Histogram analyses of the measured $E_{storage}$, E_{loss}, and loss tangent in **(C)**, **(E)** and **(G)**, respectively.

organization and cell viscoelasticity, which verify the robustness of our results.

Topography and Viscoelasticity of Cytoskeletons in Lamellipodium at pH 6.5

To study the effect of acid microenvironment on living cancer cells, we change pH value of the culture medium to pH 6.5 [22], and measure the topography and the viscoelasticity of Huh-7 cells by the improved AM-FM AFM as shown in **Figure 5** and **Supplementary Figure S3**. Unlike the homogeneous dispersion of cytoskeletons in lamellipodium at pH 7.4, the topography of **Figures 5A,B** show highly oriented and organized patterns of cytoskeletal structures at pH 6.5. The cytoskeletons are polymerized to long filaments and woven into thick bundle-like structures directed to the protruding direction of lamellipodium. The viscoelasticity, including storage modulus, loss modulus and loss tangent, of the same lamellipodium region in Huh-7 cells are measured and analyzed in **Figures 5C–H** in which the polymerized filaments and bundles are visible. The strings that have higher storage modulus, higher loss modulus and lower loss tangent than the intracellular background indicate the cytoskeletal filaments in **Figures 5C,E,G**, respectively. Interestingly, along with the convergence of cytoskeletal filaments towards the protruded lamellipodium, the storage modulus and loss modulus increase while the loss tangent decreases. The gradient of viscoelasticity in the lamellipodium region with the relationship to the cellular migration will be discussed in details in the latter section.

The histogram analyses of storage modulus, loss modulus and loss tangent were also performed as shown in **Figures 5D,F,H**, respectively. Unlike monomodal Gaussian peaks at pH 7.4, all of the storage modulus, loss modulus and loss tangent show bimodal distributions at pH 6.5, corresponding to the heterogeneous organization of cytoskeletons. In **Figure 5D** for elasticity, the lower peak of storage modulus with the mean value of ~35 kPa represents the thin and unwoven cytoskeletal filaments, while the higher peak (~60 kPa) the thick cytoskeletal filaments that have been bundled together. These results of elasticity distribution are consistent with the previous studies that the increased density of

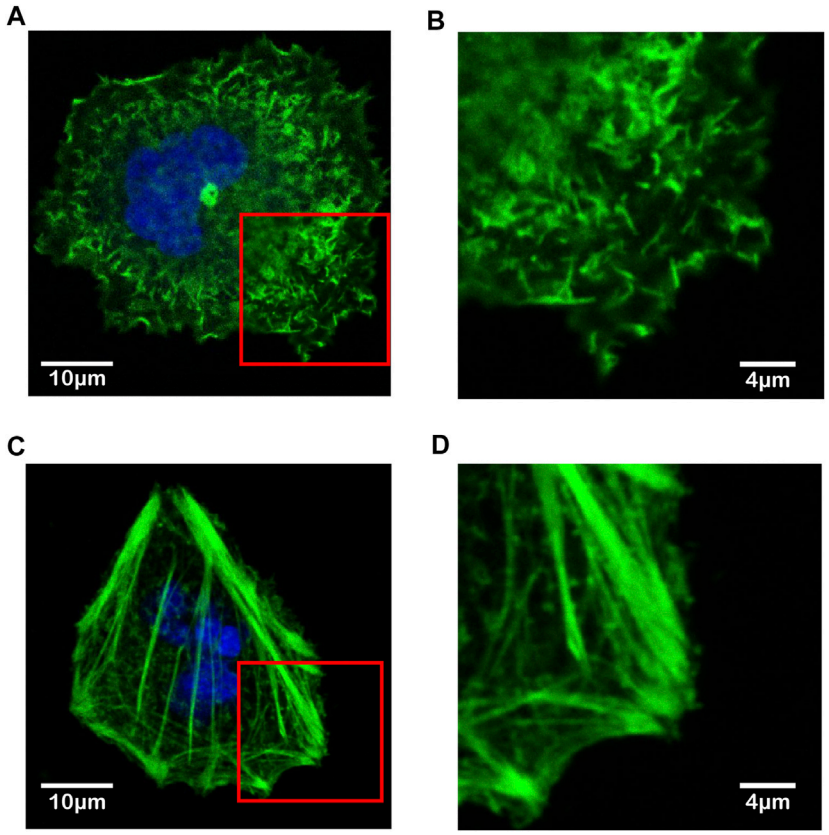

FIGURE 6 | Immunofluorescence confocal microscopy images of F-actin filaments in living Huh-7 cells under different pH microenvironments. **(A,B)** F-actin in Huh-7 cell at pH 7.4. **(C,D)** F-actin in Huh-7 cell at pH 6.5. The F-actin filaments are highlighted by green and the cell nuclei by blue. The view of **(B)** and **(D)** magnifies the rectangular region near the periphery of cell within the red box in **(A)** and **(C)**, respectively.

actin filaments can lead to the stiffening of cells [28, 29, 49]. The bundled actin filaments are bound by crosslinking proteins and molecular motor, such as fascin and myosin-X, providing strong viscosity [50, 51], which results in an elevated loss modulus as the higher peak (~40 kPa) in **Figure 5F**. Our work visualizes the organization of cytoskeletal filaments and reveals the structural origins of the viscoelasticity distribution in the lamellipodium region of living cancer cells under acid microenvironment. Repetitions of experiments for more living Huh-7 cancer cells at pH 6.5 (**Supplementary Figure S3**) show similar cytoskeleton organization and cell viscoelasticity, which verify the robustness of our results. We also performed the experiments at the pH level within the range from 6.5 to 7.4, and found that the more cells with F-actin polymerization and viscoelasticity gradient can be seen at the lower pH state.

Validation of F-Actin Cytoskeletons by Immunofluorescence Confocal Microscopy

To identify the type of cytoskeletal structures shown by the improved AM-FM AFM as in **Figures 4**, **5**, the immunofluorescence confocal microscopy was adopted and the fluorescent phalloidin that can selectively bind to F-actin was used to image the distribution of F-actin in the living Huh-7 cells (**Figure 6**) [52]. The Huh-7 cells were cultured in the two different pH environments (pH 7.4 and pH 6.5) as in AFM experiments and stained with Alexa-Fluor 488 Phalloidin and DAPI. The imaging of confocal microscopy shows that the F-actin filaments dyed by green are short, thin and randomly dispersed within the whole Huh-7 cell at pH 7.4 (**Figure 6A**). Although becoming slightly thicker near the periphery, the F-actin filaments are loosely arranged with the same homogeneous feature observed in AFM experiments (**Figure 6B**). On the contrary, at pH 6.5, the F-actin filaments that are much thicker and longer form highly oriented bundle-like structures (**Figure 6C**) and converge toward the front of lamellipodium (**Figure 6D**), which is in good agreement with the AFM imaging as well. The consistency of intercellular structures confirms that the cytoskeletal filaments visualized by the improved AM-FM AFM are the F-actin.

Viscoelasticity Gradient Facilitates Cell Adhesion and Migration

In previous sections, by using the improved AM-FM AFM, we have successfully characterized the viscoelasticity distribution of the lamellipodium regions in living Huh-7 cells at pH 7.4 and 6.5 (**Figures 4**, **5**). To compare them quantitatively, we rescale the

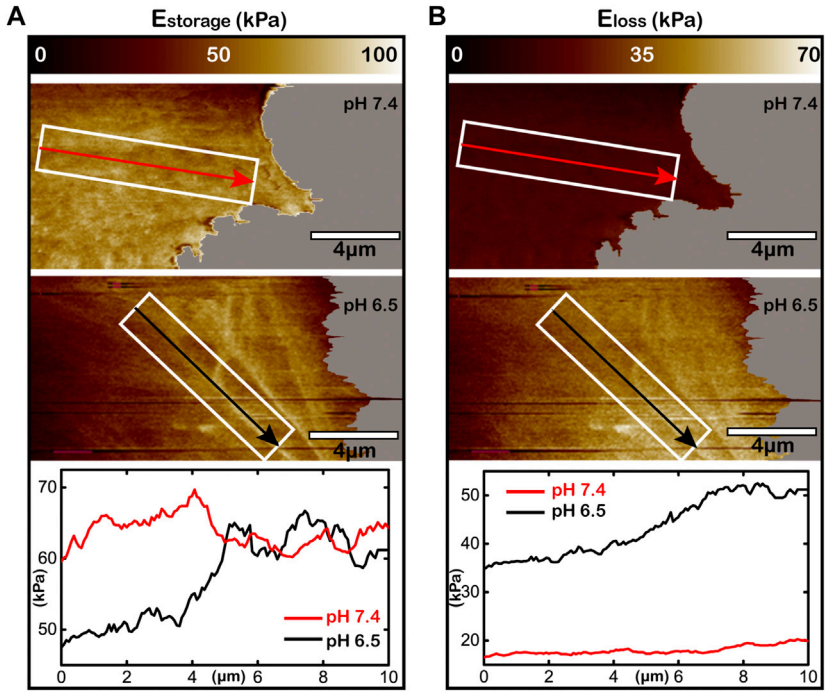

FIGURE 7 | Acid microenvironment inducing viscoelasticity gradient in the lamellipodium of living Huh-7 cells. **(A,B)** The storage modulus for elasticity **(A)** and the loss modulus for viscosity **(B)** of the lamellipodium under different pH environments. The upper panels are at pH 7.4, the middle panels are at pH 6.5, and the lower curves analyze the storage modulus or the loss modulus within the white rectangular boxes along the arrows directed to lamellipodium protrusion. The white rectangular boxes with the directions of arrows are the same for each pH value.

mapping of storage modulus (**Figure 7A**) and loss modulus (**Figure 7B**) to the same color range for studying the effect of viscoelasticity distribution on cell adhesion and migration. **Figure 7A** shows that along the direction of lamellipodium protrusion (as the arrows), the storage modulus of cell elasticity increases from ~50 kPa to over 60 kPa at the acid microenvironment and maintains at a plateau (~60 kPa) at the normal microenvironment. For cell viscosity following the same arrows, the loss modulus increases from 35 to over 50 kPa at pH 6.5, while staying at a low level of ~10 kPa at pH 7.4 (**Figure 7B**). Combining the AFM images of cytoskeletons, we can conclude that the acid microenvironment may result in the organization of F-actin filaments and the gradient of both elasticity and viscosity in living cancer cells.

Recent researches of cell migration and cancer metastasis have reported that the living cancer cells prefer to migrate toward the substrate with higher stiffness [19, 53]. However, few studies focus on the distribution and alteration of cell viscoelasticity during migration associated with the effects of cell viscoelasticity on migration. According to literatures, the higher elasticity and viscosity enable stronger adhesion to substrate [13, 54]. In our work, by using the improved AM-FM AFM, we found that the F-actin cytoskeleton aggregate and form the thick bundle-like filaments directed to the protruding direction of lamellipodium, leading to gradient increases in elasticity and viscosity. The gradient of viscoelasticity suggests a gradient of adhesion strength, which means that the lamellipodium can achieve stable adhesion at the front but have high possibility to detach the substrate at the back, resulting in the driving force for cell migration towards the direction of lamellipodium protrusion. Moreover, the aggregation and the stiffening of F-actin cytoskeleton allow focal adhesions to enhance cell adhesion, and provide sufficient cell rigidity against the forces needed for migration [55, 56]. In all, the homogeneity of F-actin cytoskeleton and viscoelasticity in the lamellipodium at pH 7.4 suppresses the migration of cancer cells, which consistent with the fact of uneasy malignant transformation of cancer cells under normal environment [47, 57]. Conversely, the aggregation of F-actin cytoskeleton and the gradient of viscoelasticity at pH 6.5 facilitate cell adhesion and migration, which explains the strong tendency in migration and metastasis of cancer cells under the acidified microenvironment in tumor tissues [47, 58]. These findings may help us to understand the structural and nanomechanical mechanism of malignant behavior of cancer cells under different pH microenvironments.

CONCLUSIONS

In summary, we have improved the original AM-FM AFM assembly, achieved the simultaneous mappings of topography and viscoelasticity of living cells under physiological conditions, and reached an ultrahigh resolution down to 50 nm for the imaging of F-actin cytoskeletons. By using the improved AM-

FM AFM, we were able to study the effect of pH microenvironment on organization of F-actin cytoskeletons and the distribution of viscoelasticity in lamellipodia of living Huh-7 cancer cells correlated with the cell adhesion and migration. The acidified environment can transform the short, thin and dispersed F-actin structures to the long, thick and oriented bundle-like structure converged along the protruding direction of lamellipodium. The conformation of F-actin cytoskeletons leads to the gradient increases of both elasticity and viscosity directed to the lamellipodium front, which provides sufficient driving force and rigidity that can facilitate cell adhesion and migration. Our work has paved the avenue for the *in situ* characterization of the F-actin microstructures and cell viscoelasticity, and contributed insights into the structural origins and nanomechanical mechanism of the migration and metastasis of living cancer cells under the acidified microenvironment.

DATA AVAILABILITY STATEMENT

The original contributions presented in the study are included in the article/**Supplementary Material**, further inquiries can be directed to the corresponding authors.

AUTHOR CONTRIBUTIONS

WZ, XZ, and YZ conceived the research. MC, WZ, XZ, ZL, and SY designed, performed, and analyzed the experiments. WZ supervised the project. MC, WZ, XZ, and YZ wrote the manuscript. All authors discussed the results and commented on the manuscript.

FUNDING

This study was supported by the National Natural Science Foundation of China (Grants 11972383 and 81827802) to WZ, by the National Natural Science Foundation of China (Grant 11672339) to YZ, by the Fundamental Research Funds for the Central Universities (Grant 19LGPY258) to WZ, and by the Natural Science Foundation of Guangdong Province, China (Grant 2021A1515010348) to WZ. The funders had no influence on study design, data collection and analysis, decision to publish or preparation of the manuscript.

ACKNOWLEDGMENTS

The experiments reported were conducted on the Physical Research Platform in School of Physics, Sun Yat-sen University (PRPSP, SYSU) and the Instrumental Analysis and Research Center, Sun Yat-sen University. We thank Teaching Center of Biology Experiment, Sun Yat-sen University for assistance with confocal fluorescence microscopy imaging.

SUPPLEMENTARY MATERIAL

The Supplementary Material for this article can be found online at: https://www.frontiersin.org/articles/10.3389/fphy.2021.674958/full#supplementary-material

REFERENCES

1. Ellinger I, and Ellinger A. Smallest Unit of Life: Cell Biology. In: E Jensen-Jarolim, editor. *Comparative Medicine Anatomy and Physiology*. Germany: Springer Press (2014). p. 19–33. doi:10.1007/978-3-7091-1559-6_2
2. Lange JR, and Fabry B. Cell and Tissue Mechanics in Cell Migration. *Exp Cel Res* (2013) 319(16):2418–23. doi:10.1016/j.yexcr.2013.04.023
3. Khalili A, and Ahmad M. A Review of Cell Adhesion Studies for Biomedical and Biological Applications. *Int J Mol Sci* (2015) 16:18149–84. doi:10.3390/ijms160818149
4. Engler AJ, Sen S, Sweeney HL, and Discher DE. Matrix Elasticity Directs Stem Cell Lineage Specification. *Cell* (2006) 126(4):677–89. doi:10.1016/j.cell.2006.06.044
5. Wei Q, Huang C, Zhang Y, Zhao T, Zhao P, Butler P, et al. Mechanotargeting: Mechanics-dependent Cellular Uptake of Nanoparticles. *Adv Mater* (2018) 30(27):1707464. doi:10.1002/adma.201707464
6. Fletcher DA, and Mullins RD. Cell Mechanics and the Cytoskeleton. *Nature* (2010) 463(7280):485–92. doi:10.1038/nature08908
7. Pollard TD, and Cooper JA. Actin, a Central Player in Cell Shape and Movement. *Science* (2009) 326(5957):1208–12. doi:10.1126/science.1175862
8. Blanchoin L, Boujemaa-Paterski R, Sykes C, and Plastino J. Actin Dynamics, Architecture, and Mechanics in Cell Motility. *Physiol Rev* (2014) 94(1):235–63. doi:10.1152/physrev.00018.2013
9. Fritzsche M, Erlenkämper C, Moeendarbary E, Charras G, and Kruse K. Actin Kinetics Shapes Cortical Network Structure and Mechanics. *Sci Adv* (2016) 2(4):e1501337. doi:10.1126/sciadv.1501337
10. Chugh P, and Paluch EK. The Actin Cortex at a Glance. *J Cel Sci* (2018) 131(14). doi:10.1242/jcs.186254
11. Oberleithner H, Callies C, Kusche-Vihrog K, Schillers H, Shahin V, Riethmüller C, et al. Potassium Softens Vascular Endothelium and Increases Nitric Oxide Release. *Proc Natl Acad Sci U S A* (2009) 106(8):2829–34. doi:10.1073/pnas.0813069106
12. Tojkander S, Gateva G, and Lappalainen P. Actin Stress Fibers - Assembly, Dynamics and Biological Roles. *J Cel Sci* (2012) 125(8):1855–64. doi:10.1242/jcs.098087
13. Li L, Zhang W, and Wang J. A Viscoelastic-Stochastic Model of the Effects of Cytoskeleton Remodelling on Cell Adhesion. *R Soc Open Sci* (2016) 3(10):160539. doi:10.1098/rsos.160539
14. Jacquemet G, Hamidi H, and Ivaska J. Filopodia in Cell Adhesion, 3D Migration and Cancer Cell Invasion. *Curr Opin Cel Biol* (2015) 36:23–31. doi:10.1016/j.ceb.2015.06.007
15. Bergert M, Chandradoss SD, Desai RA, and Paluch E. Cell Mechanics Control Rapid Transitions between Blebs and Lamellipodia during Migration. *Proc Natl Acad Sci* (2012) 109(36):14434–9. doi:10.1073/pnas.1207968109
16. Nemethova M, Auinger S, and Small JV. Building the Actin Cytoskeleton: Filopodia Contribute to the Construction of Contractile Bundles in the Lamella. *J Cel Biol* (2008) 180(6):1233–44. doi:10.1083/jcb.200709134
17. Mueller J, Szep G, Nemethova M, De Vries I, Lieber AD, Winkler C, et al. Load Adaptation of Lamellipodial Actin Networks. *Cell* (2017) 171(1):188–200. doi:10.1016/j.cell.2017.07.051
18. Bieling P, Li T-D, Weichsel J, McGorty R, Jreij P, Huang B, et al. Force Feedback Controls Motor Activity and Mechanical Properties of Self-Assembling Branched Actin Networks. *Cell* (2016) 164(1-2):115–27. doi:10.1016/j.cell.2015.11.057
19. Laurent VM, Kasas S, Yersin A, Schäffer TE, Catsicas S, Dietler G, et al. Gradient of Rigidity in the Lamellipodia of Migrating Cells Revealed by Atomic Force Microscopy. *Biophysical J* (2005) 89(1):667–75. doi:10.1529/biophysj.104.052316

20. Friedl P, and Alexander S. Cancer Invasion and the Microenvironment: Plasticity and Reciprocity. *Cell* (2011) 147(5):992–1009. doi:10.1016/j.cell.2011.11.016
21. Rofstad EK, Mathiesen B, Kindem K, and Galappathi K. Acidic Extracellular pH Promotes Experimental Metastasis of Human Melanoma Cells in Athymic Nude Mice. *Cancer Res* (2006) 66(13):6699–707. doi:10.1158/0008-5472.can-06-0983
22. Estrella V, Chen T, Lloyd M, Wojtkowiak J, Cornnell HH, Ibrahim-Hashim A, et al. Acidity Generated by the Tumor Microenvironment Drives Local Invasion. *Cancer Res* (2013) 73(5):1524–35. doi:10.1158/0008-5472.can-12-2796
23. Corbet C, and Feron O. Tumour Acidosis: from the Passenger to the Driver's Seat. *Nat Rev Cancer* (2017) 17(10):577–93. doi:10.1038/nrc.2017.77
24. Suzuki A, Maeda T, Baba Y, Shimamura K, and Kato Y. Acidic Extracellular pH Promotes Epithelial Mesenchymal Transition in Lewis Lung Carcinoma Model. *Cancer Cel Int* (2014) 14(1):1–11. doi:10.1186/s12935-014-0129-1
25. Li S, Xiong N, Peng Y, Tang K, Bai H, Lv X, et al. Acidic pHe Regulates Cytoskeletal Dynamics through Conformational Integrin β1 Activation and Promotes Membrane Protrusion. *Biochim Biophys Acta Mol Basis Dis* (2018) 1864(7):2395–408. doi:10.1016/j.bbadis.2018.04.019
26. Efremov YM, Velay-Lizancos M, Weaver CJ, Athamneh AI, Zavattieri PD, Suter DM, et al. Anisotropy vs Isotropy in Living Cell Indentation with AFM. *Sci Rep* (2019) 9(1):1–12. doi:10.1038/s41598-019-42077-1
27. Brückner BR, Nöding H, and Janshoff A. Viscoelastic Properties of Confluent MDCK II Cells Obtained from Force Cycle Experiments. *Biophysical J* (2017) 112(4):724–35. doi:10.1016/j.bpj.2016.12.032
28. Rianna C, Ventre M, Cavalli S, Radmacher M, and Netti PA. Micropatterned Azopolymer Surfaces Modulate Cell Mechanics and Cytoskeleton Structure. *ACS Appl Mater Inter* (2015) 7(38):21503–10. doi:10.1021/acsami.5b06693
29. Calzado-Martín A, Encinar M, Tamayo J, Calleja M, and San Paulo A. Effect of Actin Organization on the Stiffness of Living Breast Cancer Cells Revealed by Peak-Force Modulation Atomic Force Microscopy. *ACS Nano* (2016) 10(3):3365–74. doi:10.1021/acsnano.5b07162
30. Wang N, Zhang M, Chang Y, Niu N, Guan Y, Ye M, et al. Directly Observing Alterations of Morphology and Mechanical Properties of Living Cancer Cells with Atomic Force Microscopy. *Talanta* (2019) 191:461–8. doi:10.1016/j.talanta.2018.09.008
31. Zheludev NI. What Diffraction Limit? *Nat Mater* (2008) 7(6):420–2. doi:10.1038/nmat2163
32. Henson JH, Yeterian M, Weeks RM, Medrano AE, Brown BL, Geist HL, et al. Arp2/3 Complex Inhibition Radically Alters Lamellipodial Actin Architecture, Suspended Cell Shape, and the Cell Spreading Process. *Mol Biol Cel* (2015) 26(5):887–900. doi:10.1091/mbc.e14-07-1244
33. Svitkina TM. Platinum Replica Electron Microscopy: Imaging the Cytoskeleton Globally and Locally. *Int J Biochem Cel Biol* (2017) 86:37–41. doi:10.1016/j.biocel.2017.03.009
34. Hochmuth RM. Micropipette Aspiration of Living Cells. *J Biomech* (2000) 33(1):15–22. doi:10.1016/S0021-9290(99)00175-X
35. Peschetola V, Laurent VM, Duperray A, Michel R, Ambrosi D, Preziosi L, et al. Time-dependent Traction Force Microscopy for Cancer Cells as a Measure of Invasiveness. *Cytoskeleton* (2013) 70(4):201–14. doi:10.1002/cm.21100
36. Ayala YA, Pontes B, Ether DS, Pires LB, Araujo GR, Frases S, et al. Rheological Properties of Cells Measured by Optical Tweezers. *BMC Biophys* (2016) 9(1):1–11. doi:10.1186/s13628-016-0031-4
37. Hu S, Eberhard L, Chen J, Love JC, Butler JP, Fredberg JJ, et al. Mechanical Anisotropy of Adherent Cells Probed by a Three-Dimensional Magnetic Twisting Device. *Am J Physiol Cel Physiol* (2004) 287(5):C1184–C1191. doi:10.1152/ajpcell.00224.2004
38. Krieg M, Fläschner G, Alsteens D, Gaub BM, Roos WH, Wuite GJL, et al. Atomic Force Microscopy-Based Mechanobiology. *Nat Rev Phys* (2019) 1(1):41–57. doi:10.1038/s42254-018-0001-7
39. Haase K, and Pelling AE. Investigating Cell Mechanics with Atomic Force Microscopy. *J R Soc Interf* (2015) 12(104):20140970. doi:10.1098/rsif.2014.0970
40. Iyer S, Gaikwad RM, Subba-Rao V, Woodworth CD, and Sokolov I. Atomic Force Microscopy Detects Differences in the Surface Brush of Normal and Cancerous Cells. *Nat Nanotech* (2009) 4(6):389–93. doi:10.1038/nnano.2009.77
41. Efremov YM, Dokrunova AA, Bagrov DV, Kudryashova KS, Sokolova OS, and Shaitan KV. The Effects of Confluency on Cell Mechanical Properties. *J Biomech* (2013) 46(6):1081–7. doi:10.1016/j.jbiomech.2013.01.022
42. Kocun M, Labuda A, Meinhold W, Revenko I, and Proksch R. Fast, High Resolution, and Wide Modulus Range Nanomechanical Mapping with Bimodal Tapping Mode. *ACS Nano* (2017) 11(10):10097–105. doi:10.1021/acsnano.7b04530
43. Proksch R, and Yablon DG. Loss Tangent Imaging: Theory and Simulations of Repulsive-Mode Tapping Atomic Force Microscopy. *Appl Phys Lett* (2012) 100(7):073106. doi:10.1063/1.3675836
44. Guan D, Charlaix E, Qi RZ, and Tong P. Noncontact Viscoelastic Imaging of Living Cells Using a Long-Needle Atomic Force Microscope with Dual-Frequency Modulation. *Phys Rev Appl* (2017) 8(4):044010. doi:10.1103/PhysRevApplied.8.044010
45. Haga H, Sasaki S, Kawabata K, Ito E, Ushiki T, and Sambongi T. Elasticity Mapping of Living Fibroblasts by AFM and Immunofluorescence Observation of the Cytoskeleton. *Ultramicroscopy* (2000) 82(1-4):253–8. doi:10.1016/S0304-3991(99)00157-6
46. Webb BA, Chimenti M, Jacobson MP, and Barber DL. Dysregulated pH: a Perfect Storm for Cancer Progression. *Nat Rev Cancer* (2011) 11(9):671–7. doi:10.1038/nrc3110
47. Mogilner A, and Rubinstein B. The Physics of Filopodial Protrusion. *Biophysical J* (2005) 89(2):782–95. doi:10.1529/biophysj.104.056515
48. Guerrero CR, Garcia PD, and Garcia R. Subsurface Imaging of Cell Organelles by Force Microscopy. *ACS Nano* (2019) 13(8):9629–37. doi:10.1021/acsnano.9b04808
49. Gardel ML, Shin JH, MacKintosh FC, Mahadevan L, Matsudaira P, and Weitz DA. Elastic Behavior of Cross-Linked and Bundled Actin Networks. *Science* (2004) 304(5675):1301–5. doi:10.1126/science.1095087
50. Mattila PK, and Lappalainen P. Filopodia: Molecular Architecture and Cellular Functions. *Nat Rev Mol Cel Biol* (2008) 9(6):446–54. doi:10.1038/nrm2406
51. Rigato A, Miyagi A, Scheuring S, and Rico F. High-frequency Microrheology Reveals Cytoskeleton Dynamics in Living Cells. *Nat Phys* (2017) 13(8):771–5. doi:10.1038/nphys4104
52. Dancker P, Löw I, Hasselbach W, and Wieland T. Interaction of Actin with Phalloidin: Polymerization and Stabilization of F-Actin. *Biochim Biophys Acta* (1975) 400(2):407–14. doi:10.1016/0005-2795(75)90196-8
53. Ponti A, Machacek M, Gupton SL, Waterman-Storer CM, and Danuser G. Two Distinct Actin Networks Drive the Protrusion of Migrating Cells. *Science* (2004) 305(5691):1782–6. doi:10.1126/science.1100533
54. Yao H, and Gao H. Mechanics of Robust and Releasable Adhesion in Biology: Bottom-Up Designed Hierarchical Structures of Gecko. *J Mech Phys Sol* (2006) 54(6):1120–46. doi:10.1016/j.jmps.2006.01.002
55. Natale CF, Ventre M, and Netti PA. Tuning the Material-Cytoskeleton Crosstalk via Nanoconfinement of Focal Adhesions. *Biomaterials* (2014) 35(9):2743–51. doi:10.1016/j.biomaterials.2013.12.023
56. Qian J, Wang J, Lin Y, and Gao H. Lifetime and Strength of Periodic Bond Clusters between Elastic Media under Inclined Loading. *Biophysical J* (2009) 97(9):2438–45. doi:10.1016/j.bpj.2009.08.027
57. White KA, Grillo-Hill BK, and Barber DL. Cancer Cell Behaviors Mediated by Dysregulated pH Dynamics at a Glance. *J Cel Sci* (2017) 130(4):663–9. doi:10.1242/jcs.195297
58. Petrie RJ, Doyle AD, and Yamada KM. Random versus Directionally Persistent Cell Migration. *Nat Rev Mol Cel Biol* (2009) 10(8):538–49. doi:10.1038/nrm2729

Conflict of Interest: The authors declare that the research was conducted in the absence of any commercial or financial relationships that could be construed as a potential conflict of interest.